A near-inertial mode observed within a Gulf Stream warm-core ring

Terrence M. Joyce,[1] John M. Toole,[1] Patrice Klein,[2] and Leif N. Thomas[3]

Received 12 October 2012; revised 20 February 2013; accepted 23 February 2013; published 8 April 2013.

[1] Layering of ocean velocity "fine structure" has been coherently observed across the entire extent of a Gulf Stream warm-core ring using a shipboard acoustic Doppler current profiler system in September 2009 and independently sampled as the ring transited a moored array. Lines of constant velocity phase generally followed isopycnals as they deepened within the ring center. We also observed a clear separation of the vertical structure of the flows associated with the ring (of order 0.5 m/s) with the shorter (200 m) and less energetic (~0.2 m/s) flows of the velocity fine structure, which was further observed to rotate clockwise with increasing depth, consistent with downward propagating near-inertial waves (NIWs). Observations are consistent with a ring-scale NIW packet, probably wind forced, that shows enhanced NIW energy within the sloping pycnocline at depths of 300–700 m. Evidence of wind-forced NIWs within anticylonic eddies in a numerical simulation shows some similar features to our observations, which we try to understand physically with basic WKB-type wave/current dynamics along the lines of previously published work and a new calculation of NIW trapping within an isolated, baroclinic vortex.

Citation: Joyce, T. M., J. M. Toole, P. Klein, and L. N. Thomas (2013), A near-inertial mode observed within a Gulf Stream warm-core ring, *J. Geophys. Res. Oceans*, *118*, 1797–1806, doi:10.1002/jgrc.20141.

1. Introduction

[2] The effect of geostrophic flow on the characteristics of near-inertial waves (NIWs) highlighted by *Mooers* [1975] and *Kunze* [1985] has led to the examination of the trapping of NIWs with slightly sub-inertial frequencies within barotropic vortices [*Kunze and Boss*, 1998] and driving the enhanced vertical mixing within highly baroclinic, anticyclonic warm-core rings (WCRs) of the Gulf Stream [*Kunze et al*., 1995] and within a Taylor cap circulation above Fieberling Guyot [*Kunze and Toole*, 1997]. Trapping of NIWs by localized regions of negative vorticity arises because the effective frequency for NIWs within a quasi-axisymmetric, barotropic eddy is $\sigma_f = f + \zeta$, where $\zeta = v_{0x} - u_{0y}$, f being the usual local inertial frequency in the absence of background vorticity, and (u_0, v_0) the background geostrophic flow. As we will see, this is changed for a baroclinic eddy but the above barotropic calculation is formally valid for vertical shear and for an eddy in solid body rotation. We present some theoretical ideas concerning limiting cases of sub-inertial trapping for baroclinic, circular vortices. For anticyclonic eddies with a vertical component of vorticity of opposite sign to f, NIWs with sub-inertial frequencies are trapped within the vortex. Because of the baroclinicity of the vertical component of relative vorticity within WCRs [*Joyce*, 1984], and because of the radial component of vorticity within the vortex, the sub-inertial trapping can be vertical as well as radial, with vertical trapping due to either internal reflection or critical layer absorption. Effects of eddies on NIWs have also been studied numerically [*Young and Ben Jelloul*, 1997, *Danioux et al*., 2011], and we will draw on some numerical simulations of NIWs to understand the observations made in 2009 and reported here.

2. Observations

[3] A regular program of moored observations supported by repeated hydrography and both Shipboard and Lowered acoustic Doppler current profiler (SADCP, LADCP) sampling has been underway since spring 2004 to study the Deep Western Boundary Current (DWBC) southeast of Cape Cod. Early sections were summarized [*Joyce et al*., 2005] and guided the design of the moored array across the DWBC [*Toole et al*., 2011] called Line W. Starting in 2008, the moored array has been serviced on a 2 year interval. Between the mooring cruises, a hydrotracer cruise has been done along the line of an altimeter sub-track that defines Line W at the sea surface. During these "hydro" cruises, full-depth conductivity-temperature-depth (CTD)/LADCP sampling is typically carried out on the outbound leg out to a point close to Bermuda, and on the return, the only sampling conducted is underway SADCP measurements

[1]Woods Hole Oceanographic Institution, Woods Hole, Massachusetts, USA.
[2]Laboratoire de Physique des Océans, IFREMER, Plouzané, France.
[3]Dept. of Environmental Earth System Science, Stanford University, Stanford, California, USA.

Corresponding author: T. M. Joyce, Woods Hole Oceanographic Institution, Woods Hole, MA 02543, USA. (tjoyce@whoi.edu)

2169-9275/13/10.1002/jgrc.20141

from a 75 kHz RDI Ocean Surveyor, typically limited to the upper 700–800 m depth. Such was the case between 31 August and 10 September 2009 aboard the R/V *Endeavor* (Figure 1). Data from this cruise are augmented by observations from moored instrumentation in what we conjecture is an eddy-sized, trapped NIW packet.

[4] On the return leg, which was made without stopping for stations, underway SADCP data provide near-synoptic evidence for velocity layering (Figure 2) that extends across the entire width of the WCR. If data are smoothed by splines in the vertical and horizontal, it is possible to separate the velocity anomalies associated with the vertical banding from that of the cyclogeostrophically balanced WCR with density slowly increasing away from the ring center. So we will identify the velocity anomalies with different dynamics from ring-scale geostrophy. The sense of the rotation of the velocity anomaly down through the WCR (Figure 3) clearly indicates a clockwise rotation with depth, which is evidence for a NIW packet propagating from the surface toward the bottom [*Leaman and Sanford*, 1975]. While we show only ring center data, this rotation with depth was seen wherever the banding was present. This downward propagating NIW packet must generally have an upward phase velocity, although *Whitt and Thomas* [2012] show this is not always true. The minimum vorticity in the center of the WCR estimated from the smoothed near-surface velocity field

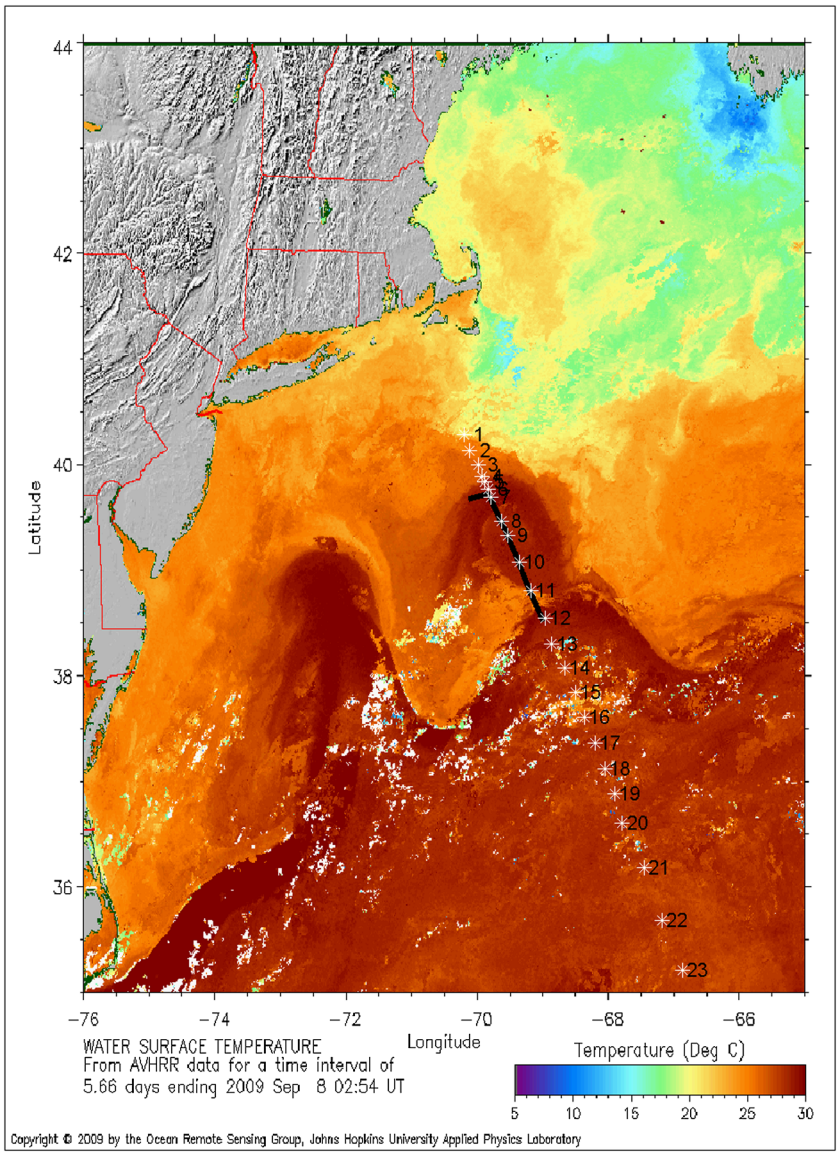

Figure 1. Stations (white asterisks with black numbers) were taken on the way south toward Bermuda (stations 24–26, off page). The return section through the WCR (mostly on 9 September 2009, about 1 week after the CTD stations in the WCR on the way south; black line) is indicated. Infrared sea surface temperature (SST) data (in color) are from *Fermi.JHUAPL*. While SST contrasts at this time of year are usually masked by broadscale warming, one can easily see the north wall of the Gulf Stream and two mostly separated warm-core rings at the crest of adjacent GS meanders. Our Line W section passed through the middle of the easternmost WCR on both legs.

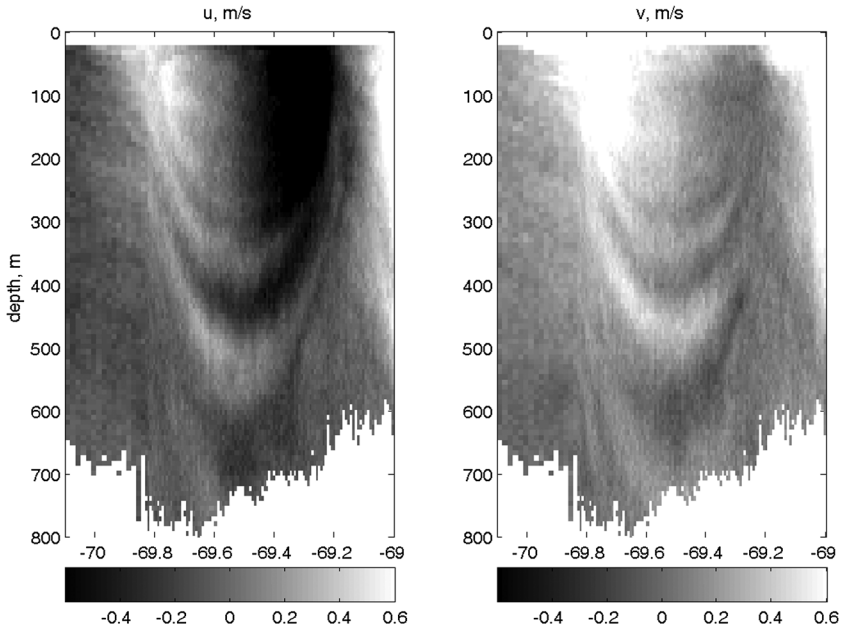

Figure 2. Grey-scale images of SADCP velocity data (zonal component on the left panel and meridional component on the right panel) plotted against longitude showing vertical banding of 100–200 m wavelength within the center of the WCR (Figure 1) with strong WSW flow on the seaward side (69.3°W) and NNW flow on the shoreward side (69.8°W). The phase of the vertical banding slopes up on both flanks of the WCR.

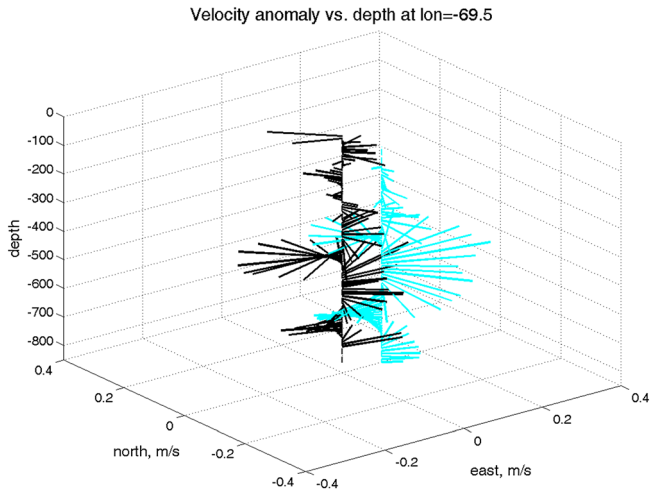

Figure 3. The anomalous (high-passed) SADCP velocity structure associated with the vertical banding near the center of the WCR (69.5°W, heavy black vectors) is plotted as a velocity anomaly hodograph versus depth. The velocity anomalies are estimated by removing a smooth spline fit to the velocity components crossing the ring having spatial scales commensurate with the WCR, not the banding, which we associated with a NIW. Mooring data (cyan) from the nearby W2 mooring, rotated forward in time (by 29 h) to be at the same phase as the SADCP profile on 9 September, have been processed to extract NIWs by combining three vertical profiles separated by half an inertial period. Mooring data have been offset 0.1 m/s in the east component and plotted above 850 m to better overlap with the SADCP data.

(Figure 4, left panel) is approximately $-0.3f$. This anticyclonic vorticity could lower the minimum frequency of the waves. As will be discussed more in detail later, the baroclinicity of the vortex, as measured by its Richardson number, $Ri_g = N^2/\left((\partial u_0/\partial z)^2 + (\partial v_0/\partial z)^2\right)$, can additionally lower the frequency of the waves by a significant amount when $Ri_g < 10$. An estimate of Ri_g will be later presented using the data from mooring W2 and reveals low values near the flanks of the eddy where there is prominent velocity fine structure (Figure 8). Here we remark that if we assume a subinertial frequency of $0.95f$, we can adjust the velocity anomalies across the WCR, which was sampled over a time period of approximately 10 h, to a fixed reference time when the vessel passed the WCR center on the return leg (±5 h). While one might quibble with the frequency choice at this stage, one must admit that time changes of ±5 h can produce significant phase changes of a NIW having a local inertial period of 18.9 h. We can reduce this aliasing by attempting to map all phases (or times) to one fixed with the center of the WCR assuming a NIW of frequency $0.95f$.

[5] Relative to the ring center, the re-mapped velocity anomalies (Figure 5, left panel) are now plotted in color together with selected potential density isopycnals from the CTD data collected on the outbound leg. The upward phase tilts of the NIW velocity anomalies nearly parallel the slope of the isopycnals, something we will consider further later. A constant phase can be followed throughout the WCR in both velocity anomaly components, which vertically can be seen to be in quadrature, consistent with a clockwise rotation of a NIW, if one moves vertically downward in the water column. The velocity anomalies are larger and their vertical scale smaller in the pycnocline ($\sigma_\theta = 26.8{:}27.0$ kg m^{-3}) than either above or below.

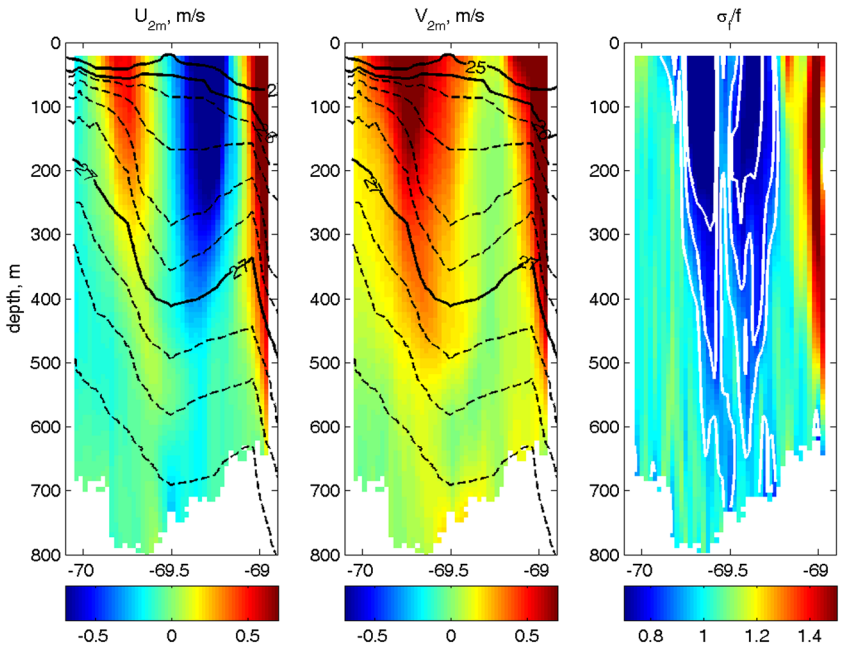

Figure 4. Smoothed velocity components and vortex-modified inertial frequency associated with the circulation of the WCR. In the latter, the white contours illustrate the sub-inertial structure of σ_f/f (equation (B10), contours of 0.75, 0.85, and 0.95), and this can be seen to encompass the region of anomalous velocities and spice (see Figure 5) within the WCR.

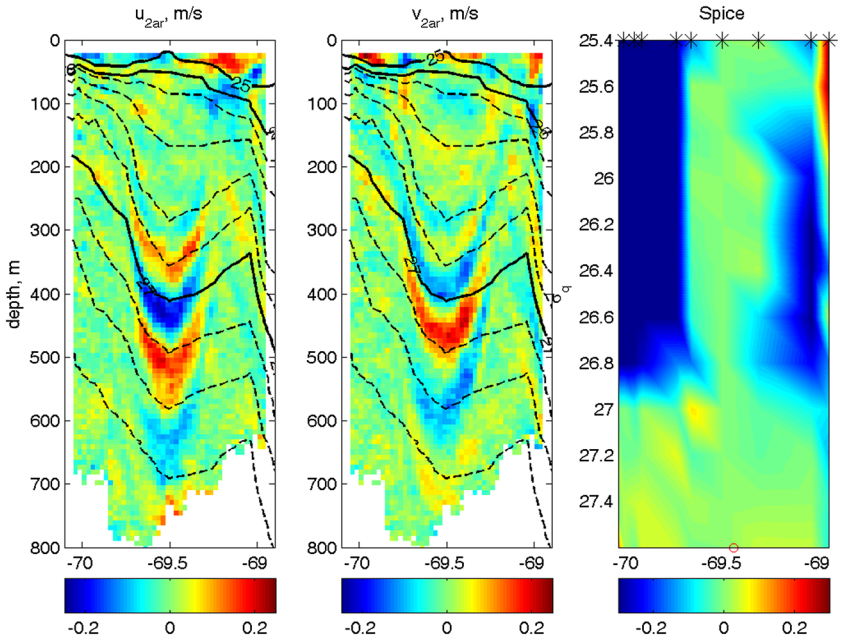

Figure 5. Phase-adjusted anomalies of velocity and spice (relative to ring center; right panel). During the velocity anomaly phase adjustment, the upward phase propagation altered the rotated velocity anomalies, and the constant phase lines (Figure 2) moved slightly upward on the right and downward on the left of ring center. Also plotted are constant σ_θ surfaces at a 0.2 kg m^{-3} contour interval. Solid lines denote the 25, 26, and 27 σ_θ surfaces. These are from the CTD stations taken on the seaward leg and have been shifted westward in longitude an amount of 0.13° to account for translation of the WCR between the two legs of the cruise. The Gulf Stream north wall can be seen intruding at the far right of all panels, consistent with the contact between the Gulf Stream and WCR indicated in Figure 1. The vertical axis is depth for the left and middle panels and σ_θ for the right panel. Longitude of the mooring W2 is indicated by the open circle at the bottom of the right panel.

[6] Between 50 and 250 m depths, a region of reduced stratification is present in the center of the ring, which is the remnant of the Eighteen Degree Water (EDW) normally found south of the Gulf Stream in the Sargasso Sea. The EDW is warmer and saltier than the corresponding water surrounding the WCR in the Slope Water region found to the north of the Gulf Stream. This water mass difference can be illustrated by plotting the spice [*Veronis*, 1972] anomaly. If α and β denote the variations of potential density with potential temperature and salinity, respectively, the spice anomaly can be written as $\delta\tau \equiv \alpha(\delta\theta) + \beta(\delta S)$, where $\delta\theta$ and δS are the potential temperature and salinity anomalies, respectively, following surfaces of constant potential density, σ_θ (Figure 5, right panel). At all depths from the surface to approximately 400 m, the waters within the core of the WCR are warmer and saltier than the surrounding Slope Water and this produces the characteristic spice anomaly signature shown. At densities $\geq 27.0\sigma_\theta$, there is little water mass contrast across the Gulf Stream and thus no apparent spice signature that would be carried across the Gulf Stream by the formation of the WCR.

[7] The WCR drifted across our Line W moored array during September, and this is documented by the mooring data from the "ring center" mooring W2, located between

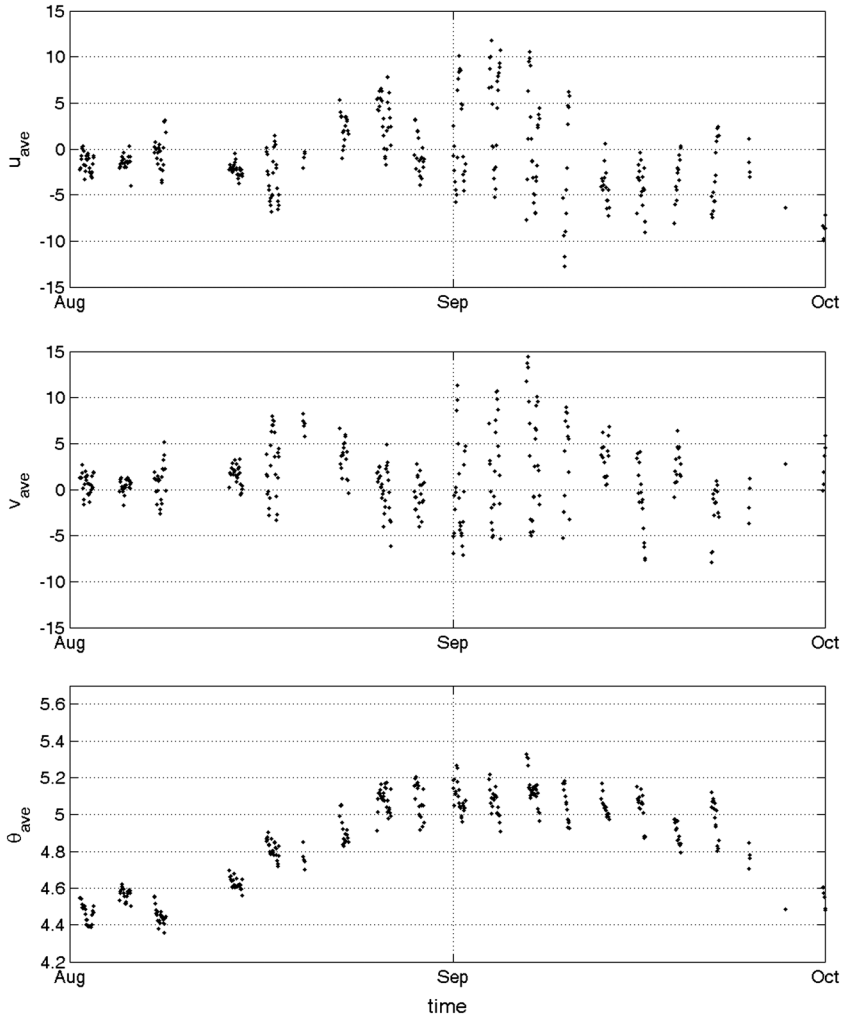

Figure 6. Mooring W2 was located just seaward of station 9, which was near the center of the WCR (Figure 1). While attempting to hold to a fixed pressure (770 dbar = 763 m) between vertical profiles, the moored profiler measured hourly currents, temperature, conductivity, and pressure from which potential temperature can be calculated. A portion of the moored time series indicates that in the first 10 days of September (2009), the profiler was in relatively warm water (°C; bottom panel) associated with the center of the WCR and measuring strong near inertial oscillations (cm/s; top and middle panels). There being no standard current meter suitably located to measure the NIWs continuously in the center of the WCR, we cannot accurately estimate the frequency of the NIWs observed at W2. However, the profiler could accurately estimate the stratification and vertical shear of the ring as it passed over the mooring site during the time interval shown. These data (see Figure 8) suggest minimum Ri_g values in the range of 3:5 in the upper 150 m on the flanks of the ring, likely lowering the minimum trapped inertial frequency a further 10:15% (equation (B9)) in these regions due to baroclinic effects.

stations 9 and 10 on our cruise (Figure 1). At this location, a McLane Moored Profiler (MMP) sampled the upper portion of the water column between 150 and 1350 decibars (1 dbar ~ 1 m) on a schedule that had it make burst of 5 one-way profiles with sampling initiated every 9.5 h (approximately half an inertial period) followed by a stationary period where it was to sit at 800 dbar making 5 min measurements every hour for 34 h, after which the profiling cycle was scheduled to begin again. The stationary data (Figure 6) from the profiler included temperature, conductivity, velocity, and pressure (pressure data not shown) time series at a nominal holding pressure of 800 dbar, just below the permanent pycnocline. Because the stationary position on the mooring line was not held by an active brake on the MMP, mooring strumming and instrument ballasting imbalances caused the profiler to slowly sink during these "stationary" periods, by an amount of about 40 m over 30 h, or approximately 0.04 cm/s. During late August, the temperature and salinity began to slowly increase, reaching a maximum around early September after which values slowly reduced. In this period of early September when the WCR was over the mooring, the velocity became highly rotary in time due to NIWs. This rotary motion was detected by the MMP while vertically profiling on mooring W2. It will be compared with the SADCP section data after adjusting the time difference in the NIW phase from the mooring (by subtracting 29 h) to make it "coincident" with that of the SADCP profile. The profiler NIW estimation was made from three successive vertical profiles separated by 9.5 h by adding the first and third profiles, subtracting twice the second profile, and dividing the result by 4, similar to that used by *Leaman and Sanford* [1975]. The agreement between the two different measures which used different platforms and methods of NIW estimation is quite remarkable (see Figure 3 again). We are unable to accurately estimate the observed frequency of the NIWs from the moored profiler during its extended stationary periods due to the slow sinking of the profiler. But one can readily estimate that a sinking speed of 0.04 cm/s and a vertical wavelength of 300 m can produce a Doppler frequency increase (for upward phase propagation) of $0.08f$, which would be significant in assessing the unshifted NIW frequency at the mooring location.

3. Numerical NIWs in an Anticyclonic Eddy

[8] Are such NIW characteristics (displayed on the left and middle panels of Figure 5) also observed in models? To answer this question, we used a high-resolution numerical simulation (fully described in *Danioux et al*. [2011]) performed with a primitive equation (PE) code. It involves a flow field exhibiting geostrophic turbulence (with a large number of mesoscale eddies) in a zonal beta-plane channel with a size of 1000 km by 2000 km and a depth of 4000 m. The resolution is 2 km in the horizontal and there are 100 levels in the vertical, with thickness varying from 3.6 m near the surface to 190 m near the bottom (4000 m) [see also *Roullet and Klein*, 2010]. The inertial period is about 18 h. The vertical profile of the mean buoyancy frequency (not shown) involves a main thermocline located at a depth around 600 m that corresponds to a first Rossby radius of deformation of approximately 30 km. The mesoscale and sub-mesoscale eddy turbulence is forced by using a relaxation to a basic state that corresponds to a large-scale meridional density gradient [see *Klein et al*., 2008 for details]. An active mixed layer (ML) with a depth of 70 m, forced by a realistic time series of high-frequency winds and surface heat fluxes, caps a seasonal thermocline whose thickness is about 40 m. The low-frequency (LF) motions (obtained after filtering motions over an inertial period) are explained by the mesoscale eddy field that derives from baroclinic instability of the basic state flow. The resulting high-frequency motions are mostly associated with near-inertial waves (NIWs). Results (from *Danioux et al*. [2011]) indicate that the presence of a fully turbulent mesoscale eddy field (involving strongly interacting eddies of different sizes) accelerates the vertical propagation of the wind-forced NIWs.

[9] The NIW features, similar to those reported above, are observed in this numerical simulation. They are found within many, but not all of the mesoscale eddies. We focus on one anticyclonic eddy, Figure 7, where NIW zonal and meridional velocities and isopycnal contours are shown. The eddy core (with a diameter of 100 km), identified by the isopycnal slopes, has a relative vorticity magnitude associated with LF motions ranging from $-0.5f$ within the ML to about $-0.2f$ at 300 m. The NIW amplitude is quite large within the mixed layer. Below the ML, NIWs are much weaker, actually 4 times smaller than the LF motions, and mostly located within the anticyclonic eddy. But their amplitude increases with depth. The phases associated with the NIW velocity components (Figures 7a and 7b) are in quadrature, consistent with the clockwise rotation with depth observed in the simulation. This indicates downward propagating waves (with therefore an upward phase velocity). Their vertical wavelength appears to be smaller just below the mixed layer and larger at depth. As in the observations described above, the constant phase lines almost parallel the

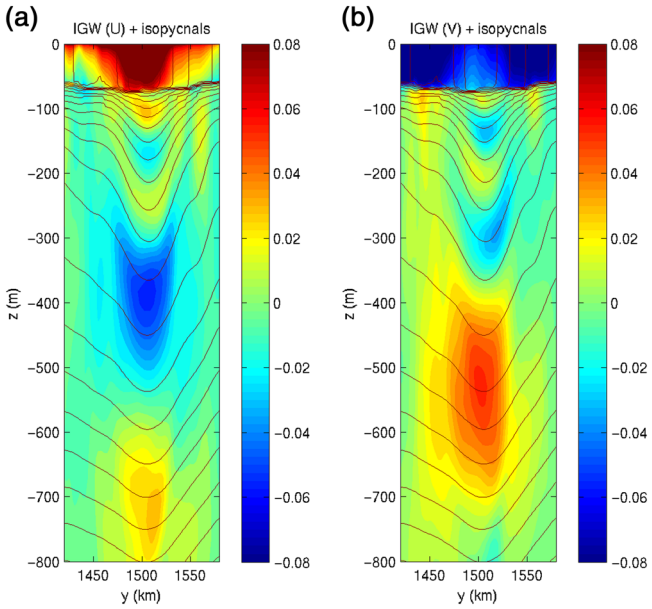

Figure 7. (a) Zonal and (b) meridional components of the NIWs observed in the numerical model. Velocities are in color (ranging from −0.08 to 0.08 m/s) and isopycnals in contours (ci = 0.06 kg/m^3).

isopycnals (actually a little steeper than the isopycnals). The isopycnal slope increases with depth down to 300 m and decreases below. The maximum isopycnal slope is associated with minimum values of geostrophic Richardson numbers $Ri_g = N^2/(\partial u_0/\partial z)^2$ of approximately 20, larger than our observation in the WCR. The highly energetic NIWs are produced in the model by the intermittent wind forcing and not by mesoscale structures experiencing unbalanced dynamics. Indeed, similar numerical simulations without wind forcing revealed very weak NIWs that quickly propagate to depth [*Danioux et al*., 2012]. These NIW characteristics (from a numerical model) are quite similar to those reported in the preceding section and can be used to answer some questions that are raised in the next section.

4. Discussion

[10] What is the source of NIWs? As mentioned above, numerical simulations with no wind forcing suggest that NIWs produced by unbalanced dynamics are very weak energetically [*Danioux et al*., 2012]. On the other hand, NIWs produced by an intermittent wind forcing have a magnitude similar to what was observed on Line W. Shipboard winds from the cruise (not centered over the WCR) reveal three strong wind events (max winds of 25 knots) occurred on approximately 2, 4, and 9 September. This suggests that the source of NIWs observed in at Line W was wind forced.

[11] To what extent were the NIWs trapped? The observed NIWs as well as those in the model indicate that velocity variability extends throughout the water column to depths of 1000 m. We have not observed (as in *Whitt and Thomas* [2012]) in the simulated eddies, any shrinking of the NIW vertical length (and therefore no critical layer) but on the contrary, vertical length appears to increase with depth, consistent with the changes in the vertical stratification. The absence of the shrinking vertical scale of the NIWs in the simulations is likely due to the high Ri_g of the vortex in contrast to the lower Ri_g values (i.e., $Ri_g < 10$) of the flows considered by *Whitt and Thomas* [2012]. The MMP data below the thermocline, however, when plotted using WKB scaling for the vertical dependence of velocity and vertical wavelength on buoyancy frequency, indicate a shrinking of the vertical scale at greater depth (not shown), which does not preclude possible critical layer dynamics from the observations within the eddy. But it is very clear that NIWs are localized (in the x,y plane) within the WCR, which seems to be an evidence for trapped NIWs.

[12] What explains the constant phase lines tilting along the isopycnal? From several analytical studies [*Mooers*, 1975; *Kunze*, 1985] and as detailed in the appendices, the eddy baroclinicity and in particular the geostrophic vertical shear act to tilt the particle orbits associated with inertial gravity waves. A heuristic explanation was suggested by *Kunze* [1985]. But a new physical interpretation has been recently proposed by *Whitt and Thomas* [2012]. These physical arguments are offered for a 2-D situation, such as NIWs near a strongly baroclinic zonal front.

[13] Within a baroclinic, circular WCR, we encounter a situation which has not been studied to our knowledge. We therefore present an analysis of NIWs within a baroclinic vortex (Appendix B) which shows that the minimum inertial frequency becomes $\sigma_{\min} = \left[\sigma_f^2 - f^2 Ri_g^{-1}\right]^{\frac{1}{2}}$, where $\sigma_f = \sqrt{\left(f + \frac{2u_0}{r}\right)(f + \zeta_0)}$, and u_0, ζ_0, and Ri_g are the azimuthal flow, vertical vorticity, and geostrophic Richardson number of the background vortex flow, respectively. The latter can afford a trapping mechanism for NIWs within the pycnocline in regions of reduced Ri_g. Our data (Figure 8) suggest that as the WCR passed over the mooring, regions of lowest Ri_g were located on the flanks of the ring in the upper 150 m. This would mainly enhance the region of trapping radially relative to what is plotted in Figure 4 (right panel), where this effect could not be directly estimated.

[14] However, this can be estimated using the data from the CTD section, which we shall now do. In Figure 5, one can see a large lateral gradient of spice on the western side of the WCR near a longitude of $-69.7°$. This is a region with robust NIW signals and moderate shear. We use the shifted CTD data to estimate the geostrophic Richardson Number and the SADCP data the remaining terms of (B9). At this location (Figure 9), we can see that the effect of stratification as measured by Ri_g is reducing the minimum NIW frequency limit ($\sigma_{\min}$) below σ_f. However, the major baroclinic structure in the trapping is due to the increase in the vorticity and circulation near the ocean surface. It is clear that the additional vertical trapping due to Ri_g is not affecting the location of the oscillatory signals (Figure 9, right panel) and that the NIW is not at its theoretical minimum frequency limit. Finally, the flow is dominantly geostrophic as indicated by the similarity of the Richardson numbers derived from the spline-smoothed ADCP vertical shear and that from the CTD stations bounding the front.

[15] In this theory, the velocity anomalies are aligned along isopycnals for the lowest NIW frequency and are assumed axisymmetric. However, the observed anomalies have constant phases which seem to tilt more than the isopycnals on the side in contact with the Gulf Stream (GS), which could be an artifact caused by the noncontemporaneous SADCP and CTD measurements and the evolution of the eddy and the GS. Moreover, we remark that eastward and northward velocity anomalies for an axisymmetric perturbation would show sign reversals across the ring, which are not observed (in the ocean or the model as presented here). What we observe is more like an azimuthal mode 1 disturbance, again suggesting a frequency somewhat higher than the low-frequency limit. But with one observational section, our sampling cannot determine the modal structure and our theoretical arguments provide limiting constraints which cannot be expected to apply in detail.

[16] We believe that imaging of a coherent, ring-scale NIW packet using acoustics as described here is novel in that we have employed a readily interpretable Doppler signal indicative of velocity layering. We note that there is an observable, but not as pronounced, layering signal in the backscattered amplitude on our SADCP section through the warm-core ring. Other, low-frequency "seismic" methods have previously been successful at imaging fine structure on the scale of rings and eddies [e.g., *Holbrook et al*., 2003] where the signal is not as readily interpretable as a Doppler shift but is generally thought to be due to temperature/density fine structure. It is possible that our observed NIW packet might also contain structures that could be imaged by these seismic techniques, including density-related fine structure

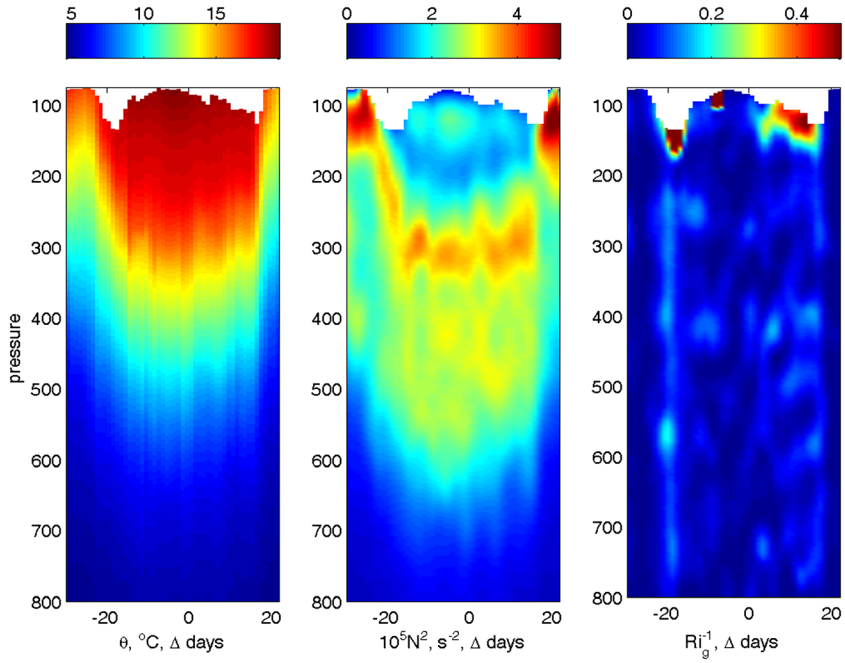

Figure 8. Mooring W2 profiles of basic variables allowed a section of Ri_g to be estimated over the 52 day period of transit of the warm-core ring over the mooring. Vertical shear and buoyancy frequency were smoothed by a 20 m boxcar filter and used to estimate Ri_g. In the three panels, we show potential temperature (°C), buoyancy frequency squared (s^{-2}), and Ri_g^{-1} as a time series for days relative to the ring center data plotted earlier (Figure 3). The Eighteen Degree Water core of the WCR with low stratification between 150 and 200 dbar/m depth/pressure is anomalous for the region to the north of the Gulf Stream except for WCRs. The high-stratification region below this layer can be seen to deepen 200 m during the WCR passage. Regions of low Ri_g are most prominent near the flanks of the WCR in the upper ocean where strong currents often prevent profiler sampling.

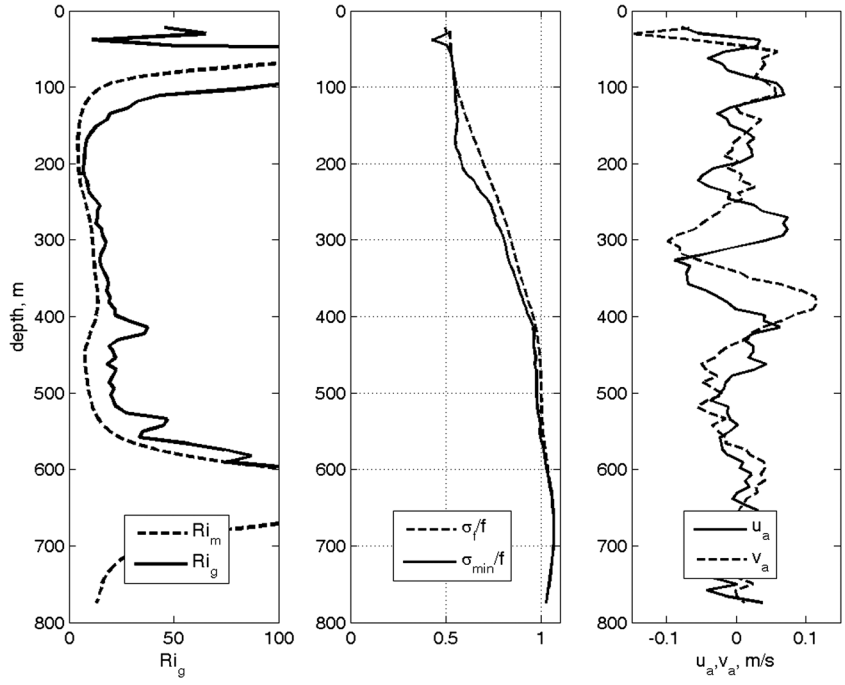

Figure 9. We use CTD-derived stratification and SADCP-derived, spline-smoothed data to estimate the vertical shear and the mean Richardson number (Ri_m) for the CTD stations bounding the deep spice front near longitude = −69.7°. Assuming geostrophy and using the radial density gradient provide a geostrophic estimate (Ri_g, left panel). The two limiting trapping frequencies using Ri_g are scaled by f (middle panel) and plotted with the velocity anomalies (east and north) as a function of depth at this location (right panel).

associated with the advection field of the NIW packet. But these structures would, if present, be propagating vertically, and not fixed to or necessarily aligned with particular density surfaces. We hope that future studies may combine the two types of sampling, but we recognize the intermittency of the NIW signal due to wind stress variability is a formidable barrier to overcome.

Appendix A: Impact of Isopycnal Slope on the Dispersion of Near-Inertial Gravity Waves

[17] The arguments quickly developed below essentially come from the material detailed in *Mooers* [1975] in a 2-D non-hydrostatic framework and later discussed in a 3-D hydrostatic framework with low Rossby number by *Kunze* [1985, equation (7) and section 3b]. They allow us to understand the relationship between the NIW phase lines and the isopycnal slope (induced by the baroclinicity of a geostrophic flow) in terms of the NIW wave vector and frequency. It should be noted that Mooers' ideas have been extended in a recent study by *Whitt and Thomas* [2012] inspired by Gulf Stream ADCP observations, much like our own case. This approach will be extended here (in Appendix B) by application to a cylindrical coordinate system more appropriate to a ring.

[18] We define $N^2 = b_{0z}$ the square of the buoyancy frequency and $M^2 = b_{0x} = fv_{0z}$ the 2-D (x,z) geostrophic vertical shear in thermal wind balance. $b_0 = -g\rho/\rho_0$ is the buoyancy and v_0 the meridional velocity. The subscript "0" refers to the geostrophic flow, assumed to be entirely meridional. The slope of the isopycnals is given by $s = -M^2/N^2$. The effective Coriolis frequency is defined as $\sigma_f = [f(f+v_{ox})]^{1/2}$, and $\psi(x,z,t)$ is the stream function associated with the NIWs whose frequency, σ, is assumed to be much smaller than N:$\sigma \ll N$. We focus on the lines of constant phase of NIWs classically defined as $-k/m$ (with k and m, respectively, the horizontal and vertical wave numbers) and compare them with the slope of the isopycnals, s.

[19] Moving to a hydrostatic framework and using the linearized PEs (wave-wave interactions being dropped out and using the 2-D geostrophic flow), the dispersion relation derived by *Mooers* [1975, equation (12)] reduces to

$$\psi_{xx} - 2s\psi_{xz} - \frac{\left(\sigma^2 - \sigma_f^2\right)}{N_2}\psi_{zz} = 0, \tag{A1}$$

which, after moving to a spectral space and using the WKB approximation, leads to

$$-\frac{k}{m} = s \pm \left(s^2 - s_c^2 + \frac{\sigma^2}{N^2}\right)^{1/2} \tag{A2}$$

(with $s_c^2 = \sigma_f^2/N^2$):

[20] For propagating waves, the radicand in equation (A2) must be positive. This implies the existence of a minimum frequency given by

$$\sigma_{\min}^2 = \sigma_f^2 - f^2 Ri_g^{-1} \tag{A3}$$

with Ri_g a Richardson number defined as $Ri_g = f^2N^2/M^4$ (see [*Whitt and Thomas*, 2012]), explicitly pointing out the importance of baroclinicity to inertial wave trapping. It should be noted that the solution $\sigma = \sigma_{\min}$ leads (from (A2)) to $-k/m = s$, indicating that particle orbits exactly line up with the isopycnals.

[21] When NIW phase lines do not exactly line up with the isopycnals ($-k/m \neq s$), the solution for σ (from equation (A2)) can be written as

$$\sigma^2 = \sigma_f^2 + N_{\text{eff}}^2\left(\frac{k}{m}\right)^2, \quad N_{\text{eff}}^2 \equiv N^2\left(1 + 2s\frac{m}{k}\right), \tag{A4}$$

[22] As discussed in *Kunze* [1985] (who derived the 3-D version), N_{eff} can be interpreted as an effective buoyancy frequency felt by the wave. It depends on the orientation of the wave vector k/m with respect to that of the density gradient vector s. If N_{eff} is smaller (larger) than N, waves behave more (less) inertially. One interesting solution (with $k \neq 0$) is that NIWs with frequency close to the effective Coriolis frequency should have constant phases almost lined up with (but steeper than) the isopycnal slope, corresponding to $-k/m \sim 2s$.

[23] These results point out that the minimum frequency given by equation (A3) may allow one to better understand the impact of the baroclinicity on the NIW trapping. Furthermore, the comparison between the constant phase lines of NIWs and the slope of isopycnals may provide some estimation (although heuristic) of the observed NIW frequency (using equation (A4)).

Appendix B: Impact of a Baroclinic, Circular Vortex on Inertial Wave Trapping

[24] We are unaware of a derivation for the minimum frequency of inertia-gravity waves in a baroclinic, circular vortex so it is presented here using parcel arguments similar to those described in *Whitt and Thomas* [2012]. The vortex satisfies the gradient wind and hydrostatic balances:

$$-\frac{{u_0}^2}{r} - fu_0 = -\frac{1}{\rho_0}\frac{\partial p_0}{\partial r} \tag{B1}$$

$$b_0 - \frac{1}{\rho_0}\frac{\partial p_0}{\partial z} = 0 \tag{B2}$$

where u is the azimuthal velocity, r is the radial distance from the center of the vortex, p is the pressure, $b = -g\rho/\rho_0$ is the buoyancy, and the subscript "0" denotes that the variable is associated with the balanced vortex. Combining (B1) and (B2) to form the thermal wind balance for the vortex yields

$$\left(f + \frac{2u_0}{r}\right)\frac{\partial u_0}{\partial z} = \frac{\partial b_0}{\partial r} \equiv M^2 \tag{B3}$$

[25] The vortex is perturbed by a disturbance that has no azimuthal variations, with velocity components (u',v',w') and displacements $\delta r = \int_0^t v'dt'$ and $\delta z = \int_0^t w'dt'$. The disturbances yielding the minimum frequency correspond to perturbations that are purely along isopycnals, i.e., $\delta z = -(M^2/N^2)\delta r$. Such perturbations do not generate buoyancy or pressure

anomalies, and therefore their dynamics are governed by the radial momentum equation:

$$\frac{Dv'}{Dt} - \left(f + \frac{2u_0}{r}\right)u' = 0, \tag{B4}$$

where it has been assumed that the strength of the perturbation flow is much weaker than the balanced flow, i.e., $u' \ll u_0$. The azimuthal momentum equation for the total flow, $u = u' + u_0$; $v = v'$,

$$\frac{Du}{Dt} + \frac{uv}{r} + fv = 0 \tag{B5}$$

is simply an expression of angular momentum conservation, i.e., $fr^2/2 + ur = \text{const}$ following the fluid parcels. This conservation principle can be used to determine u' in terms of parcel displacements and properties of the balanced flow. Assume that the parcel starts at a position (r_1, z_1) where the balanced flow is equal to u_{o1} and $u' = 0$ and that it is displaced to the location $(r_2 = r_1 + \delta r;\ z_2 = z_1 + \delta z)$ where the background flow is equal to u_{o2} and the perturbed flow is u', v'. It follows from angular momentum conservation that

$$u'r_2 = u_{01}r_1 - u_{02}r_2 - f/2\left(r_2^2 - r_1^2\right) \tag{B6}$$

[26] Assuming small parcel displacements, the balanced flow can be expanded using a Taylor series $u_{02} \approx u_{01} + (\partial u_0/\partial r)\delta r + (\partial u_0/\partial z)\delta z$, and neglecting second-order terms (e.g., terms like $u'\delta r$), it follows

$$u' \approx -(f + \zeta_{01})\delta r - (\partial u_0/\partial z)\delta z \tag{B7}$$

where $\zeta_0 = (1/r)\,\partial(ru_0)/\partial r$ is the vertical vorticity of the balanced vortex. For parcel displacements that are along isopycnals, (B7) becomes

$$u' \approx -\left(f + \zeta_{01} - \frac{M^4}{(f + (2u_{01}/r))N^2}\right)\delta r, \tag{B8}$$

where the thermal wind balance (B3) has been used. Substituting (B8) into (B4) and recalling the relationship between v' and δr yield an equation for simple harmonic motion of along-isopycnal motion with a frequency given by

$$\sigma_{\min} = \left[\sigma_f^2 - f^2 Ri_g^{-1}\right]^{\frac{1}{2}}, \tag{B9}$$

where $Ri_g = N^2 f^2/M^4$ is the Richardson number of the balanced flow, and the "effective" inertial frequency is given by

$$\sigma_f = \sqrt{\left(f + \frac{2u_0}{r}\right)(f + \zeta_0)}. \tag{B10}$$

[27] Note that this differs from that for a barotropic vortex [*Kunze and Boss*, 1998] in that baroclinic effects are included in Ri_g and the vertical vorticity dependence is different unless the ring is in solid body rotation, which we have not assumed here. For values of Ri_g of O(10), the minimum frequency of NIWs can be reduced by baroclinicity an additional 5% below the effective inertial frequency.

[28] **Acknowledgments.** Initial observations at Station W (2001–2004) were made possible by a grant from the G. Unger Vetlesen Foundation and support from the Woods Hole Oceanographic Institution. Since 2004, the Line W program (http://www.whoi.edu/science/PO/linew/) has been supported by the U.S. National Science Foundation with supplemental contribution from WHOI's Ocean and Climate Change Institute. We wish to thank Frank Bahr, Jane Dunworth-Baker, and Leah Trafford for assistance with the data and plots presented in this work. PK is supported by IFREMER and CNRS (France). The simulations reported here were performed on the Earth Simulator (Yokohama, Japan) through a MOU between IFREMER and JAMSTEC. LNT was supported by the National Science Foundation grant OCE-0961714.

References

Danioux, E., P. Klein, M. W. Hecht, N. Komori, G. Roullet, and S. Le Gentil (2011), Emergence of wind-driven near-inertial waves in the deep ocean triggered by small-scale eddy vorticity structures, *J. Phys. Oceanogr.*, *41*(7), 1297–1307. http://dx.doi.org/10.1175/2011JPO4537.1

Danioux, E., J. Vanneste, P. Klein, and H. Sasaki (2012), Spontaneous inertia gravity-wave generation by surface-intensified turbulence, *J. Fluid Mech.*, *699*, 153–173. Publisher's official version: http://dx.doi.org/10.1017/jfm.2012.90

Holbrook, W. S., P. Páramo, S. Pearse, and R. W. Schmitt (2003), Thermohaline fine structure in an oceanographic front from seismic reflection profiling, *Science*, *301*, 821–824.

Joyce, T. M. (1984), Velocity and hydrographic structure of a Gulf Stream warm-core ring, *J. Phys. Oceanogr.*, *14*(5), 936–947.

Joyce, T. M., J. Dunworth-Baker, R. S. Pickart, D. Torres, and S. Waterman (2005), On the Deep Western Boundary Current south of Cape Cod, *Deep-Sea Res. II*, *52*, 615–625.

Klein, P., B.-L. Hua, G. Lapeyre, X. Capet, S. Le Gentil, and H. Sasaki (2008), Upper ocean turbulence from high-resolution 3D simulations, *J. Phys. Oceanogr.*, *38*(8), 1748–1763. http://dx.doi.org/10.1175/2007JPO3773.1

Kunze, E. (1985), Near-inertial wave propagation in geostrophic shear, *J. Phys. Oceanogr.*, *15*, 544–565.

Kunze, E., R. W. Schmitt, and J. M. Toole (1995), The energy balance in a warm-core ring's near-inertial critical layer, *J. Phys. Oceanogr.*, *25*, 942–957.

Kunze, E., and J. M. Toole (1997), Tidally driven vorticity, diurnal shear, and turbulence atop Fieberling Seamount, 1997, *J. Phys. Oceanogr.*, *27*(12), 2663–2693.

Kunze, E. and E. Boss (1998). A model for vortex-trapped internal waves, *J. Phys. Oceanogr.*, *28*, 2104–2115.

Leaman, K., and T. Sanford (1975), Vertical energy propagation of internal waves: A vector spectral analysis of velocity profiles, *J. Geophys. Res.*, *80*, 1975–1978.

Mooers, C. N. K. (1975), Several effects of a baroclinic current on the cross-stream propagation of inertial-internal waves. *Geophys. Fluid Dynam.*, *6*, 245–275.

Roullet, G., and P. Klein (2010), Cyclone-anticyclone asymmetry in geophysical turbulence, *Phys. Rev. Lett.*, *104*(21), 1–4.

Toole, J. M., R. G. Curry, T. M. Joyce, M. McCartney, and B. Peña-Molino (2011), Transport of the North Atlantic deep western boundary current about 39°N, 70°W: 2004–2008, *Deep-Sea Res. II*, doi:10.1016/j.dsr2.2010.10.058.

Veronis, G., 1972. On properties of seawater defined by temperature, salinity and pressure. *J. Mar. Res. 30*, 227–255.

Whitt, D. B., and L. N. Thomas (2012), Near-inertial waves in strongly baroclinic currents, *Am. Meteorol. Soc.*, doi:10.1175/JPO-D-12-0132.1.

Young, W. R., and M. Ben Jelloul (1997), Propagation of near-inertial oscillations through a geostrophic flow, *J. Mar. Res.*, *55*, 735–766.